ACS Catalysis

pubs.acs.org/acscatalysis Research Article

Active Palladium Structures on Ceria Obtained by Tuning Pd−Pd Distance for Efficient Methane Combustion

Weiwei Yang, Haohong Song, Lihua Zhang, Junyan Zhang, Felipe Polo-Garzon, Haodong Wang, Harry Meyer, III, De-en Jiang,* Zili Wu,* and Yuanyuan Li*

Cite This: ACS Catal. 2024, 14, 16459−16468 Read Online

ACCESS | Metrics & More | Article Recommendations | Supporting Information

ABSTRACT: Efficiently removing/converting methane via methane combustion imposes challenges on catalyst design: *how to design local structures of a catalytic site so that it has both high intrinsic activity and atomic efficiency*? By manipulating the atomic distance of isolated Pd atoms, herein we show that the intrinsic activity of Pd catalysts can be significantly improved for methane combustion via a stable Pd_2 structure on a ceria nanorod support. Guided by theory and confirmed by experiment, we find that the turnover frequency (TOF) of the Pd_2 structure with the Pd−Pd distance of 2.99 Å is higher than that of the Pd_2 structure with the Pd−Pd distance of 2.75 Å; at least 26 times that of ceria supported Pd single atoms and 4 times that of ceria supported PdO nanoparticles. The high intrinsic activity of the 2.99 Å Pd−Pd structure is attributed to the conductive local redox environment from the two O atoms bridging the two Pd^{2+} ions, which facilitates both methane adsorption and activation as well as the production of water and carbon dioxide during the methane oxidation process. This work highlights the sensitivity of catalytic behavior on the local structure of active sites and the fine-tuning of the metal−metal distance enabled by a support local environment for guiding the design of efficient catalysts for reactions that highly rely on Pt-group metals.

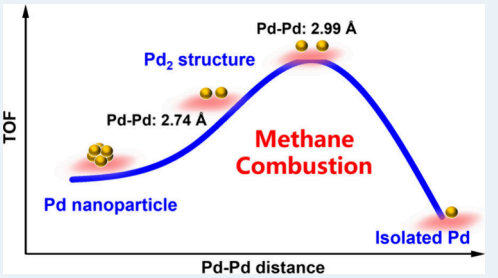

KEYWORDS: *Pd_2 structure, tune Pd−Pd distance, Pd single atoms, methane combustion*

1. INTRODUCTION

Catalytic methane (CH_4) to carbon dioxide (CO_2) is industrially significant in addressing unburnt CH_4 emission issue from natural gas-powered vehicles and other heating sources.[1−3] Fundamentally, methane combustion is used as a model reaction for developing active structures that can efficiently activate and convert kinetically stable methane at a low energy cost.[4−7] Among all studied catalysts, oxide-supported Pd catalysts have shown superior activity in converting CH_4 to CO_2 and hence attracted much attention in determining the nature and structure of active Pd species for developing highly reactive catalysts with a minimum dependence on critical platinum group elements.[4,8−10] The key question to be addressed is, *what are the key features of the active Pd species/sites for methane combustion*?

To address this question, previous reports have been focused on revealing the oxidation states of the active Pd species. However, contradictory results are often reported. For instance, in some reports, Pd^{2+} was proposed to be the active centers, while Pd^{4+} was inactive over Pd/ceria catalysts.[11] Some other work, however, suggested that the Pd^{4+} site, mixed or partially embedded in the ceria lattice, offered lower methane activation barriers in comparison to Pd^{2+} states.[12−14] Recently, a few groups proposed that the active Pd catalyst likely comprised mixed Pd species with different chemical states (Pd^0-core−PdO-shell particles, Pd^0/Pd^{2+} combination, or mixed Pd^{2+} and Pd^{4+}).[15−18] These seemingly contradicting results imply that the chemical state of Pd may not be the primary descriptor for determining the catalytic performances of the Pd catalyst for methane combustion.

Instead of the oxidation states of the Pd species, the local atomic structure of Pd sites could play a decisive role in activating and converting methane. For instance, Cui et al. showed that Pd^{2+} in PdO nanoparticles embedded inside or on the surface of zeolite framework were more active than the finely dispersed Pd^{2+} sites.[5] Our recent work suggested that Pd^{4+} single atom species with different local atomic structures could coexist in a Pd/ceria catalyst, and the one that could transform into $Pd^{\delta+}$ ($0 < \delta < 2$) single atom sites with a defective bonding environment was responsible for the drastically improved activity.[19] Despite efforts in tuning supports or interactions between supports and isolated Pd atoms, these previous studies showed that the activity of Pd single atoms were much less than those of PdO particles.[5,19,20] The remaining question is then, *how to design a robust Pd*

Received: August 19, 2024
Revised: October 12, 2024
Accepted: October 13, 2024

https://doi.org/10.1021/acscatal.4c04985
ACS Catal. 2024, 14, 16459−16468

structure exhibiting both high atomic efficiency and enhanced intrinsic activity.

In an active structure, Pd sites could be in an under-coordinated local bonding environment, enabling unique interactions with methane and providing the lowest energy barrier for the initial dissociation adsorption of methane.[6,21−26] Furthermore, in an active structure, both Pd−O interaction and Pd−Pd interactions could be important since calculations showed that the presence of an oxygen atom directly below the coordinatively unsaturated Pd atom in the two-layer PdO (101) film was crucial for efficient methane dissociation, and density functional theory (DFT) also suggested that the Pd−Pd dimer could show better catalytic performance compared with Pd single atoms and PdO.[21,27] These results prompt us to *hypothesize* that a robust Pd structure exhibiting both high atomic efficiency and enhanced intrinsic activity can be obtained by manipulating the atomic distances of isolated Pd atoms on oxide supports.

In this work, theoretical calculations and experiments are combined to test this hypothesis. Specifically, first, DFT and microkinetic modeling are applied to determine possible stable Pd−Pd structures with different proximities supported on ceria, provide insights into their reaction mechanisms, and identify the Pd structures that potentially show enhanced catalytic activity for methane combustion. Second, to test the predictions from the DFT and microkinetic modeling, ceria supported Pd sites with different Pd−Pd atomic distances are prepared by controlling the local surface density of Pd single atoms on ceria and characterized by combining multiple techniques, including X-ray photoelectron spectroscopy (XPS), X-ray absorption spectroscopy (XAS), and scanning transmission electron microscopy (STEM). The intrinsic activity of these samples is determined by performing steady-state isotopic transient kinetic analysis (SSITKA) and compared with those of ceria supported Pd single atoms and PdO particles. Our results from both theory and experiment underscore the significance and promise of a proper proximity between Pd single atoms for optimum reactivity in methane combustion.

2. METHODS

2.1. Catalyst Preparation. All chemicals were purchased from Sigma-Aldrich. The ceria nanorod (NR) was synthesized following a modified procedure reported elsewhere.[28] Typically, 360 mmol of NaOH was mixed with 3.8 mmol of $Ce(NO_3)_2{\cdot}6H_2O$ and 0.2 mmol of $ZrO(NO_3)$ in 60 mL of deionized water (D.I.). The addition of a small amount of Zr helps improve the stability of ceria NR. After stirring at room temperature for 30 min, the solution was transferred to a 100 mL Teflon liner and sealed in a stainless-steel autoclave. The autoclave was put in a 100 °C oven and held for 24 h to obtain NR. After cooling to room temperature, the precipitates were collected by D.I. washing for several times until the pH equaled 7−8 and then dried overnight at 80 °C. The NR was calcined at 550 °C for 3 h in static air for further use.

Pd−Ce series catalysts with varying weight loadings (1, 3, 5, and 8 wt %) of Pd were prepared by using a conventional wetness impregnation method.[11,29] In brief, a certain amount of Pd precursor solution containing tetraamminepalladium(II) nitrate (TAPN) was mixed with the above obtained ceria powders, followed by drying at 80 °C overnight. The resulting mixture was then calcined at 800 °C for 10 h in flowing air. The high temperature calcination resulted in a ceria surface dominated with the (111) facet.[19,30] Depending on the different loading amounts of Pd and the local structure of Pd species, the catalysts were termed as 1Pd, 3Pd, 5Pd, or 8Pd catalyst.

2.2. Characterizations. Nitrogen physisorption at 77 K was performed using a TriStar II Plus 3.03 instrument. Prior to measurement, 100 mg of the used sample was degassed at 150 °C for 6 h. The Brunauer−Emmert−Teller method was then adopted to analyze the surface area. Powder X-ray diffraction (XRD) patterns were obtained using a PANalytical X'Pert Prosystem with Cu Kα (λ = 0.15406 nm) radiation at 45 kV and 40 mA. The Raman spectra were obtained via a customized ellipsoidal mirror and directed by a fiber optics bundle to the spectrograph stage of a triple Raman spectrometer (Princeton Instruments Acton Trivista 555). Edge filters (Semrock) were used in front of the UV−vis fiber optic bundle (Princeton Instruments) to block laser irradiation. The 325 nm (10 mW at sample) excitation laser is generated from a HeCd laser (Melles Griot). A UV-enhanced liquid N_2-cooled CCD detector (Princeton Instrument) was employed for signal detection. Atomic-resolution high angle annular dark-field scanning transmission electron microscopy (HAADF-STEM) was carried out on an aberration-corrected Hitachi HD2700C STEM operated at 200 kV. The Pd/ceria samples were dispersed onto carbon-coated copper grids after sonication in ethanol. The Pd content was determined by using inductively coupled plasma optical emission spectrometry with a Spectroblue (AMETEK Inc.) instrument. X-ray photoelectron spectroscopy (XPS) measurements were performed for catalysts by using a Thermo K-Alpha XPS system with a spot size of 400 μm and a resolution of 0.1 eV. X-ray absorption spectroscopy (XAS) measurements were performed at Beamline 7-BM (QAS) of the National Synchrotron Light Source II, Brookhaven National Laboratory. For the ex situ measurement, the sample powders were spread onto Kapton tape, which was then folded and sealed. Pd K-edge XAS data were collected in fluorescence mode. The obtained XAS data were processed and analyzed by using the Demeter package.[31]

The concentrations of Pd−Pd ensembles in the spent 3Pd and 5Pd catalysts are estimated. Based on XPS results (as shown in later figures), both Pd single atoms and Pd−Pd ensembles take 2+ oxidation states. Among Pd^{2+} single atom sites and Pd−Pd ensembles, the concentration of Pd−Pd ensembles in 3Pd (5Pd) is estimated to be $0.114 \le x_3 \le 0.69$ ($0.182 \le x_5 \le 0.77$) and x_3 (x_5) is defined as the concentration of Pd−Pd ensembles in the spent 3Pd (5Pd) catalyst. Here are the details of the estimation. Since the Pd^{2+} and Pd^{4+} single atom sites coexist in the fresh samples and with the increase of the reaction temperature, the concentration of Pd^{4+} decreases, while that of Pd^{2+} increases; the increased Pd^{2+} ensembles must be converted from Pd^{4+} single atom sites and can also be converted from Pd^{2+} single atom sites. Assuming it is only converted from Pd^{4+} single atom sites, we can obtain the minimum concentration of Pd−Pd ensembles in the spent 3Pd and 5Pd samples. That would be 11.4% Pd−Pd ensembles in the spent 3Pd and 18.2% Pd−Pd ensembles in the spent 5Pd sample. Assuming that, in the spent samples, all Pd^{2+} species are Pd−Pd ensembles, the maximum concentration of Pd−Pd ensembles will be 69% in the spent 3Pd and 77% in the spent 5Pd sample. Therefore, based on XPS, the concentration of Pd−Pd ensembles in 3Pd (5Pd) is estimated to be $0.114 \le x_3 \le 0.69$ ($0.182 \le x_5 \le 0.77$). In fact, the ranges of x_3 and x_5 can be further narrowed. For instance, for the spent 5Pd catalyst,

https://doi.org/10.1021/acscatal.4c04985
ACS Catal. 2024, 14, 16459−16468

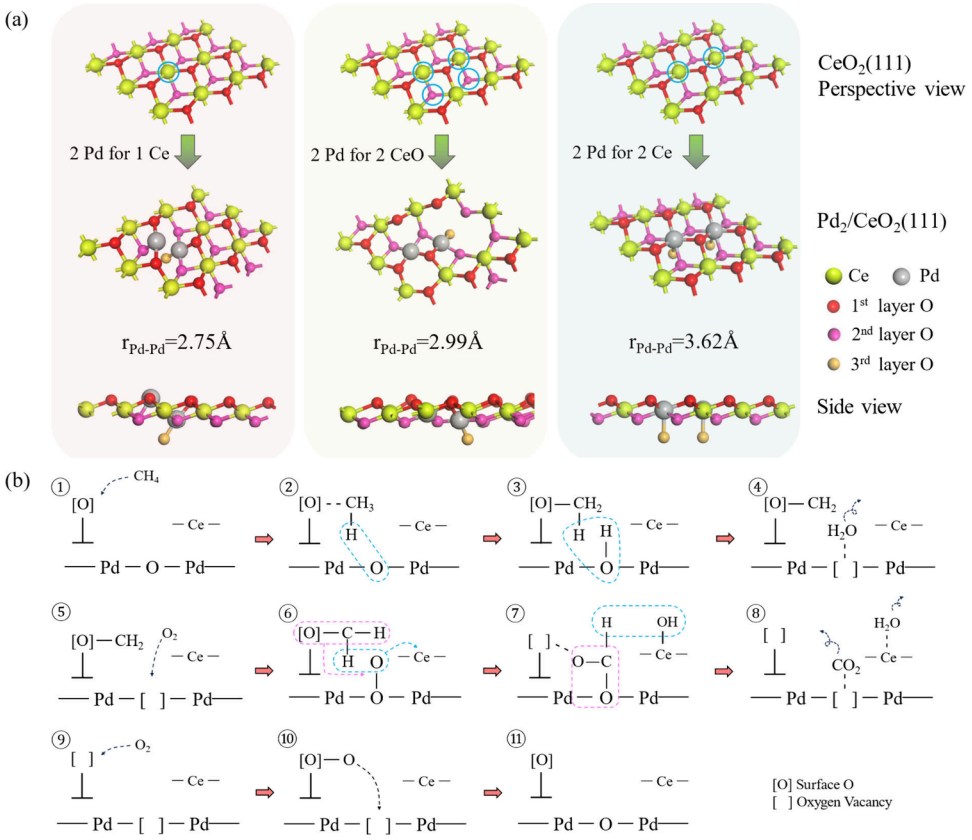

Figure 1. Pd dimers on the $CeO_2(111)$ surface and the methane oxidation pathway on the 2.99 Å Pd_2/CeO_2 from DFT calculations. (a) Three most stable Pd_2 structures on the $CeO_2(111)$ surface and how they are derived. (b) Schematic reaction pathway for the complete oxidation of methane on the 2.99 Å Pd_2/CeO_2 model.

the coordination number of Pd−Pd is about 1.6 and it is defined as the total number of Pd−Pd bonds divided by the total number of Pd atoms.[32,33] If x_5 = 0.2, since only Pd ensembles contribute to Pd−Pd bonds, the Pd−Pd coordination number needs to be corrected to 8, which corresponds to a Pd cluster with a size about 1.7 nm (assuming a hemispherical cuboctahedral structure of the cluster).[34,35] However, such clusters are not detected by STEM. Based on the combined XAS and XPS results, we estimate that the concentration of Pd−Pd ensembles in 3Pd (5Pd) is within the range of $0.3 \leq x_3 \leq 0.69$ ($0.3 \leq x_5 \leq 0.77$).

2.3. Activity Measurement. The catalyst activity was evaluated in a vertical fixed-bed reactor (inner diameter of 4 mm) that was installed in a commercial Altamira Instruments system (AMI system, mBenchCAT). The sample was mixed with quartz sand at a mass ratio of 1:10, which was packed between quartz wool plugs in the tube reactor. For the light-off and light-out curves of CH_4 oxidation over 3Pd, 5Pd, and 8 Pd catalysts, to ensure the Pd amount was the same for each measurement, the catalyst amount was determined to be 34.2, 20, and 12.8 mg for 3Pd, 5Pd, and 8Pd, respectively. A gas mixture consisting of 0.5% CH_4 and 2.5% O_2 in He was fed onto the sample, with an interval of 25 °C/50 °C between neighboring measurement points stepwise heating from 300 up to 700 °C, or the reverse, at a ramp rate of 5 °C/min. The total flow rate was 20 mL/min. Correspondingly, the GHSV ((mL/g_{cat})/h) should be 35087, 60000, and 93750 for 3Pd, 5Pd, and 8Pd, respectively. At each temperature point during the light-off, the reaction was held for at least 1 h to obtain a steady conversion. The effluent gases were analyzed by online gas chromatography over a SRI 8610C GC.

Steady-state isotopic transient kinetic analysis (SSITKA) is a useful experimental technique that provides information about surface kinetic parameters, such as surface residence time, surface concentration of intermediates, and turnover frequencies during steady-state reaction conditions.[36,37] The transient switch from an unlabeled $^{12}CH_4$ to a labeled $^{13}CH_4$, or the reverse (i.e., $^{13}CH_4 \rightarrow {}^{12}CH_4$), leads to the replacement of unlabeled (labeled) surface intermediates by the labeled (unlabeled) ones without altering the steady-state conditions of the reaction (assuming the molecular mass and vibrational characteristics of the labeled and unlabeled species are similar) when the reaction has arrived at steady state. Generally, the time difference spent between the inert Ar tracer and the CO_2 response indicates the mean surface residence time (τ) of the whole reaction (CH_4 /O_2 diffuse → adsorb → activation → transient state → CO_2 product → desorb) and the concentration of intermediates on the surface.

In this work, the mean surface residence time (τ) is calculated based on the integration area between the normalized transient response of CO_2 product and that of the inert Ar tracer (see the examples in the Supporting Information), as shown below,

$$\tau(s) = \int_0^t [F^{CO_2}(t) - F^{Ar}(t)]\, dt$$

The area corresponds to the mean surface time spent for CH_4 to form CO_2 in the reactive pathway over the surface. Real mean surface time (τ_0) of reaction intermediates can be

https://doi.org/10.1021/acscatal.4c04985
ACS Catal. 2024, 14, 16459−16468

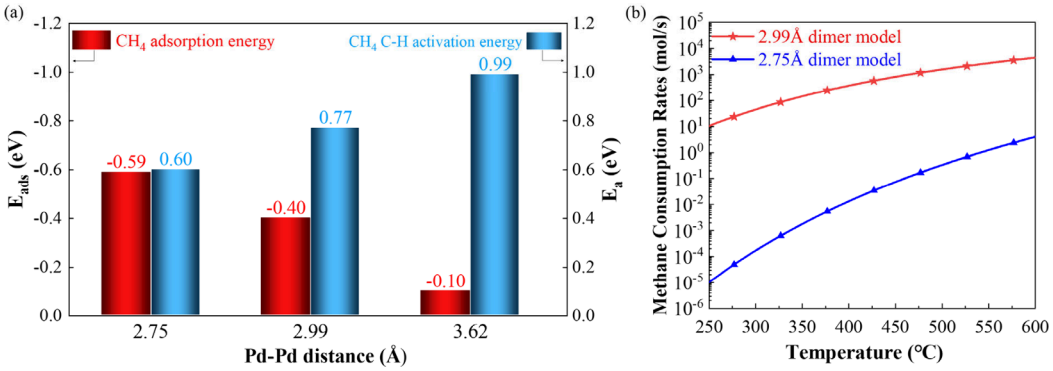

Figure 2. Comparison of the Pd_2 models on the CeO_2 (111) surface for methane oxidation. (a) DFT-computed energetic differences in CH_4 adsorption energy and C−H activation energy. (b) Microkinetic modeling of the $CH_4 + 2O_2 \rightarrow CO_2 + 2H_2O$ reaction on the 2.75 and 2.99 Å Pd_2 models on CeO_2 based on the DFT energy profiles in Figure S3.

obtained by extrapolating the τ at different flow rates to zero contact time, as displayed in Figures S1 and S2 in the Supporting Information. The turnover frequency (TOF) is hence obtained from τ_0 via the following equation assuming pseudo-first-order reaction with a single-intermediate pool.[37]

$$\mathrm{TOF} = \frac{1}{\tau_0}$$

2.4. DFT Calculations and Microkinetic Modeling. Density functional theory (DFT) calculations were performed using the Vienna ab initio simulation package (VASP).[38,39] The Perdew−Burke−Ernzerhof (PBE)[40] functional of generalized-gradient approximation (GGA) was used for electron exchange and correlation. The on-site Coulomb interaction was included using the DFT+U method and a U value of 4.5 eV was used for Ce following previous studies.[41−43] The electron−core interaction was described using the projector-augmented wave method (PAW).[44,45] The kinetic energy cutoff was set to 500 eV for the plane wave basis set. For the calculations of Pd dimers/CeO_2 (111), we used a periodic slab with a (4 × 4) supercell and the Brillouin zone was sampled using the 3 × 3 × 1 k-mesh. The CeO_2 (111) slab model is four Ce−O−Ce layers thick, and the vacuum thickness was set to 15 Å. The atoms in the bottom two layers were frozen to their bulk position and only the top two Ce−O−Ce layers were allowed to relax. Transition states were found using the climbing-image nudged elastic band method[46] and the dimer method[47] with the force convergence criterion of 0.05 eV $Å^{-1}$. The MKMCXX code was used for microkinetic modeling.[48] The reaction rates and rate-controlling steps via degree-of-rate-control (DRC) analysis[49,50] were investigated to compare the performances of the two different Pd dimers.

3. RESULTS AND DISCUSSION

3.1. Prediction of Pd−Pd Configurations for CH_4 Combustion. To create the local environment most beneficial for methane combustion, our guiding principle is to manipulate the Pd−Pd distance to tune the local environment through Pd−Pd, Pd−O−Pd, and Pd−O−Ce interactions. DFT geometry optimizations followed by ab initio molecular dynamics simulations at 700 K were performed to elucidate the possible Pd−Pd configurations that are stable on CeO_2. The CeO_2 (111) was chosen as the active surface according to its thermodynamic stability among typical ceria surfaces.[51] By exploring close to 20 Pd_2 configurations on CeO_2 (111) via add-on (Table S1), substitution (Table S2), and mixed add-on/substitution (Table S3) modes of model generation, we identified three stable Pd−Pd configurations in the substitution mode with distinctly different Pd−Pd distances: 2.75, 2.99, and 3.62 Å (Figure 1a). For simplicity, hereafter, "2.75/2.99/3.62 Å structure" is used to name a Pd_2 structure obtained by tuning Pd−Pd distance, which changes not only the Pd−Pd distance but also the local electronic and atomic structures. Specifically, in the 2.75 Å structure (Figure 1a, left), two Pd^{2+} ions are next to each other with one on the surface and the other in the subsurface and no bridging O; this model was also found in a previous computational study.[27] The 2.99 Å structure, which has not been previously reported, is obtained by substituting two Pd^{2+} ions for two $(CeO)^{2+}$. The resulting structure has two bridging O ions between the two Pd^{2+} ions and the Pd−Pd distance is 2.99 Å (Figure 1a, middle). In the 3.62 Å structure, two adjacent Ce atoms were substituted by two Pd atoms, this isovalent substitution does not result in a significant surface reconstruction (Figure 1a, right). The oxidation states of Pd in the Pd_2 structures are further confirmed by comparing the Bader charges with that in bulk PdO and PdO_2 (Table S4).

To examine whether these three stable Pd−Pd structures would show different catalytic performances in methane oxidation, we first calculated the CH_4 adsorption energy and the first C−H activation energy. As one can see from Figure 2a, the 3.62 Å Pd−Pd structure has both weak methane adsorption and a high C−H activation energy, while both the 2.75 and 2.99 Å Pd_2 structures look promising. We further mapped out the complete methane oxidation pathways on the 2.75 and 2.99 Å Pd_2 structures (Figure S3). Although they share similar first two dehydrogenation steps, the key mechanistic difference between the two structures is the early participation of a bridging O atom in the 2.99 Å Pd_2 structure, which leads to facile water formation, followed by O_2 activation (Figure 1b), while on the 2.75 Å Pd_2, O_2 gets activated first before water formation (Figure S3). The comparison revealed a key advantage of the 2.99 Å Pd_2 structure where the bridging O atoms between the two Pd atoms can be more easily activated and reduced; the oxygen vacancies between the two Pd atoms are also where O_2 gets activated (Figure 1b). This is further supported by the lower oxygen vacancy formation energy on the 2.99 Å Pd_2 structure (Table S5).

To further differentiate the catalytic activities of the 2.75 and 2.99 Å Pd_2 models for methane combustion, which are not immediately clear from the DFT energy profiles given their

https://doi.org/10.1021/acscatal.4c04985
ACS Catal. 2024, 14, 16459−16468

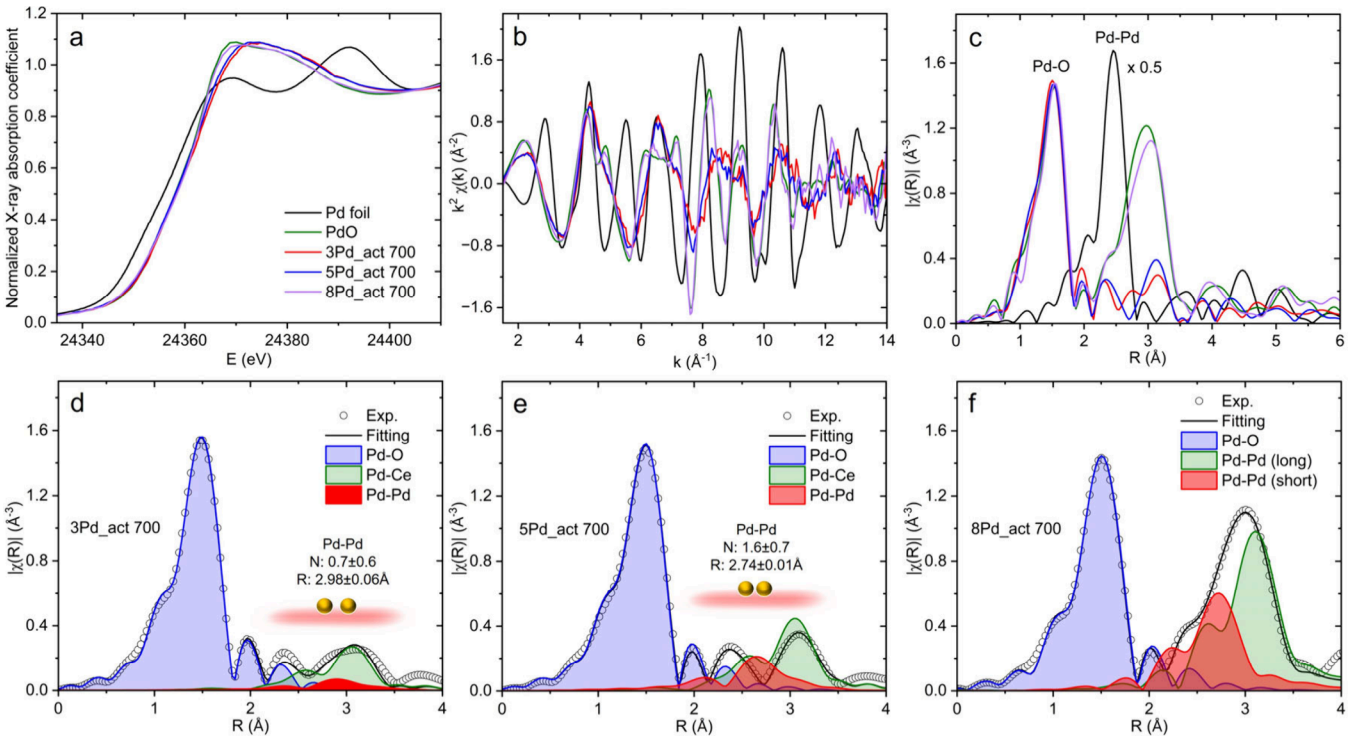

Figure 3. Local atomic structures of Pd in (3, 5, 8) Pd samples. (a) Pd K edge XANES, (b) k-space, and (c) R-space EXAFS spectra of the spent 3Pd, 5Pd, and 8Pd catalysts. For comparison, the spectra of Pd foil and PdO are included. Panels b and c share the same label as in panel a. The comparison of experimental and the fitted spectrum of (d) spent 3Pd, (e) 5Pd, and (f) 8Pd catalysts. Panels d, e, and f also include the contributions of individual fitting paths for references.

mechanistic differences, we performed microkinetic modeling based on the DFT energy profiles. As compared in Figure 2b, the 2.99 Å Pd−Pd model shows a higher activity for the temperature range examined. In addition, analysis of the degree of rate control (Figure S4) indicates that the rate-determining step for the 2.99 Å model is the first C−H activation (TS1) and dissociation of second adsorbed O_2 (TS5), while, on the 2.75 Å model, the rate is strongly limited by the second water desorption,[27] which is 1.40 eV uphill (last step in Figure S3). In contrast, the desorption energy of water is low on the 2.99 Å model (<0.5 eV).

3.2. Generation and Structure Determination of Pd−Pd Structures with Different Distances. The above theoretical results along with previous computational studies show that the intrinsic activity of the 2.99 Å Pd−Pd structure is higher than that of the 2.75 Å Pd−Pd structure, and both are more active than Pd single atoms and PdO counterparts.[27] To test the theoretical findings, a series of Pd/CeO_2 samples are prepared. To control the distance of the Pd single atoms, we gradually increased the weight loading of Pd atoms on ceria. Such an idea was also implemented by Kwak et al., who constructed 2D Pt rafts on the γ-Al_2O_3 surface by adjusting Pt loadings.[52] In addition, we found that when the weight loading of Pd was 1 wt %, Pd single atoms remained isolated throughout the reaction of methane combustion.[19] Therefore, in this work, we change the weight loading of Pd to 3, 5, and 8 wt % and these samples are correspondingly labeled as 3Pd, 5Pd, and 8Pd hereafter.

To determine the local structure of Pd in 3Pd, 5Pd, and 8Pd catalysts, Pd K-edge XAS spectra are collected. It is very likely that the as-prepared catalysts or even the pretreated catalysts will go through species/structure modifications under reaction conditions (which will also be demonstrated in the later section of this work).[19,43] We therefore focus on the spent and stable catalysts (collected after methane combustion at the highest temperature of 700 °C). Figure 3 shows the XANES and EXAFS spectra of the spent 3Pd, 5Pd, and 8Pd catalysts. As shown in Figure 3a, for the XANES spectra of all samples, the position of the rising edge is similar to that of PdO, suggesting that in all three samples Pd is in an oxidized state. For the spent 8Pd catalyst, the XANES (Figure 3a) and EXAFS (Figure 3b,c) spectra are close to those of PdO, indicating that the PdO phase is formed and dominated in the spent 8Pd catalyst. On the other hand, the XAS spectra of the spent 3Pd and 5Pd are quite different from those of PdO and Pd foil, suggesting that, in the spent 3Pd and 5Pd catalysts, Pd atoms have local structures different from those in PdO and Pd particles. By comparing the spectra of the spent 3Pd and 5Pd, subtle changes can also be observed. Specifically, the maxima (at about 24372 eV) of the XANES spectrum shifts slightly toward lower energy for the spent 5Pd catalyst. In the EXAFS spectra of the spent 3Pd and 5Pd catalysts, different features can be observed in the range 8−10 $Å^{-1}$ in the *k*-space (Figure 3b) and in the range 2.0−3.5 Å in the *R*-space (Figure 3c).

To identify the reasons for the observed spectral changes and obtain quantitative local structure information, EXAFS analysis is performed. For the spent 8Pd catalyst, since its spectrum is similar to that of PdO (based on the raw data examination discussed above), the paths of Pd−O, Pd−Pd (short), and Pd−Pd (long) that are extracted from the crystal structure of PdO are included in the fitting model. In fitting the spectra of the 3Pd and 5Pd catalysts, the model includes three paths: Pd−O, Pd−Pd, and Pd−Ce. The comparison of the experimental spectra and the fitted spectra and the

https://doi.org/10.1021/acscatal.4c04985
ACS Catal. 2024, 14, 16459−16468

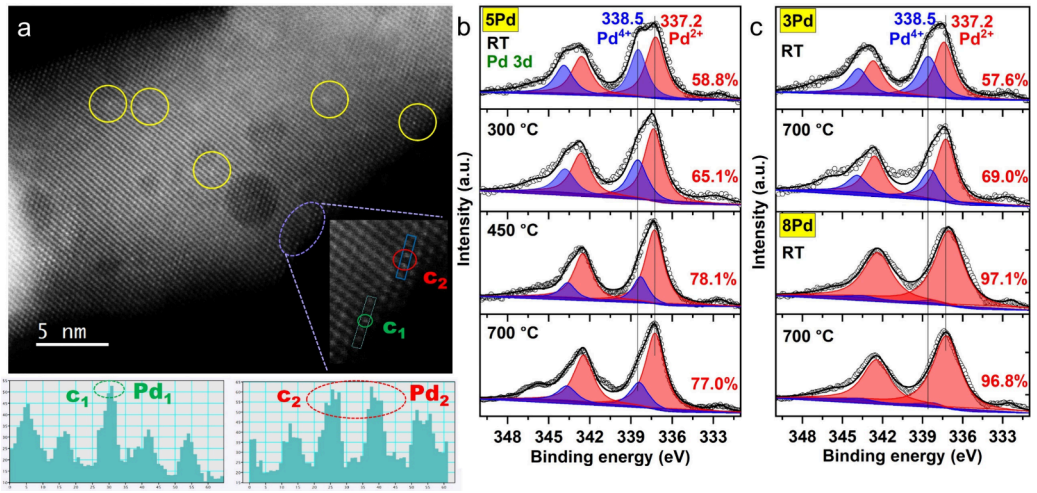

Figure 4. Local distribution and electronic properties of Pd species. (a) Representative STEM image of the spent 5Pd catalyst. More images can be found in Figure S5. Inset shows the presence of both single (c_1) and dimer (c_2) Pd atoms on crystalline ceria. (b) Pd 3d XPS spectra (scatter) of the as prepared 5Pd catalyst and the 5Pd catalyst after the methane combustion at 300, 450, and 700 °C. (c) Pd 3d XPS spectra (scatter) of the as prepared and spent (after reaction at 700 °C) 3Pd and 8Pd catalysts. For panels b and c, the fitted spectra and the contribution of Pd^{2+} and Pd^{4+} species are included for references. The Pd^{2+} concentrations obtained from peak fittings are also listed next to the corresponding spectra.

contribution of each path are plotted in Figure 3d,e,f. The fitting k range is 2.0−12.0 $Å^{-1}$, and the fitting R range is 1.0−3.5 Å. The amplitude reduction factor (S_0^2 = 0.79 ± 0.05) is obtained by fitting the spectrum of PdO. The best fitting results are summarized in Table S6.

Based on the fitting results, in addition to the dominant Pd−O contribution, a small Pd−Pd contribution (the Pd−Pd coordination number is 0.7 ± 0.6) can be detected in the spent 3Pd catalyst. The distance of this Pd−Pd path is 2.98 ± 0.06 Å, similar to that of the nearest Pd−Pd path in PdO (3.01 ± 0.01 Å)[19] and similar to that in the theoretical 2.99 Å Pd−Pd model (Figure 1a, middle). Compared to the spent 3Pd catalyst, a higher coordination number (1.6 ± 0.7) of Pd−Pd bond is obtained for the spent 5Pd catalyst and the Pd−Pd bond distance is shorter (2.74 ± 0.01 Å), close to that of the nearest Pd−Pd path in Pd foil (2.740 ± 0.002 Å) and that in the theoretical 2.75 Å Pd−Pd model (Figure 1a, left). The obtained small Pd−Pd coordination numbers imply that the Pd ensembles in the spent 3Pd and 5Pd catalysts are very small, further confirmed by the STEM images of the spent 5Pd catalyst, as shown in Figure 4a and Figure S5. Based on the images collected on the multiple areas of the catalyst, only isolated Pd atoms and very small Pd ensembles can be detected, agreeing with the XAS results. In addition, as shown in Figure S6, no Pd or PdO species can be observed in the XRD patterns of the spent 3Pd and 5Pd samples, again suggesting the small sizes of Pd species in these samples. For the spent 8Pd catalyst, as expected, the local structure is similar to that of PdO, consisting of a short Pd−Pd (the nearest) path at a distance of 3.01 ± 0.02 Å and a long Pd−Pd (the second nearest) path at a distance of 3.41 ± 0.01 Å. The obtained coordination numbers of Pd−Pd paths (2.3 ± 0.7 for the short Pd−Pd and 5.4 ± 1.5 for the long Pd−Pd) for the spent 8Pd catalyst are smaller than those in PdO (4.0 for the short Pd−Pd and 8.0 for the long Pd−Pd), suggesting nanosized PdO in the spent 8Pd catalyst. This is also supported by the weak diffraction peak of PdO (reference code 04-005-4781) in the XRD patterns (Figure S6). These quantitative results of Pd−Pd coordination numbers and Pd−Pd distances for the spent 3Pd, 5Pd, and 8Pd catalysts reflect that by increasing the weight loading of Pd, we indeed drive the pairing of Pd atoms and the formation of Pd ensembles with different Pd−Pd distances that are in good agreement with the DFT predicted models.

In fact, in addition to the increased surface density, another required driving force for the generation of Pd−Pd structures in the spent 3Pd and 5Pd catalysts is the reaction condition, which increases the mobility of Pd atoms. Figure S7 shows the Pd K-edge XAS spectra of the as prepared 3Pd and 5Pd catalysts, and based on the analysis (Table S6), the Pd−Pd pairs barely exist in the as-prepared catalysts, suggesting that isolated Pd single atoms dominate in the as-prepared 3Pd and 5Pd catalysts and the small Pd ensembles (Pd pairs) are only created during the reaction at elevated temperatures. Accompanied by the developed Pd−Pd pairs in the spent 3Pd and 5Pd catalysts is the redistribution of oxidized Pd species on the surface of catalysts. Figure 4b shows the Pd 3d XPS spectra of the as-prepared and post-reaction 5Pd catalysts. At room temperature (RT), Pd^{2+} (~337.2 eV) and Pd^{4+} (~338.6 eV) species coexist in the as-prepared 5Pd catalyst.[16,53,54] With the increase of the reaction temperature (RT to 450 °C), the concentration of Pd^{2+} species increases and the concentration of Pd^{4+} decreases. Further increasing the temperature to 700 °C, the concentrations of Pd^{4+} and Pd^{2+} remain almost unchanged. The temperature-dependent increase of Pd^{2+} species is also observed in the 3Pd catalysts (Figure 4c). These XPS results, when combined with those obtained from XAS, suggest that Pd atoms in the developed Pd ensembles in the spent 3Pd and 5Pd catalysts are in an oxidation state of +2 and they originate from the conversion of certain Pd^{4+} and/or Pd^{2+} single atom species that pre-exist in the as-prepared 3Pd and 5Pd catalysts. For the 8Pd catalyst, it is dominated with Pd^{2+} (Figure 4c) in the as-prepared and spent catalysts, agreeing with XAS results that the as-prepared and spent 8Pd catalysts are primarily comprised of PdO particles (Figure 3, Figure S7, and Table S6).

All of these results indicate that by tuning the weight loading of Pd atoms on the ceria support and by controlling the external environments, Pd−Pd structures with different distances can be obtained. Furthermore, the experimentally

https://doi.org/10.1021/acscatal.4c04985
ACS Catal. 2024, 14, 16459−16468

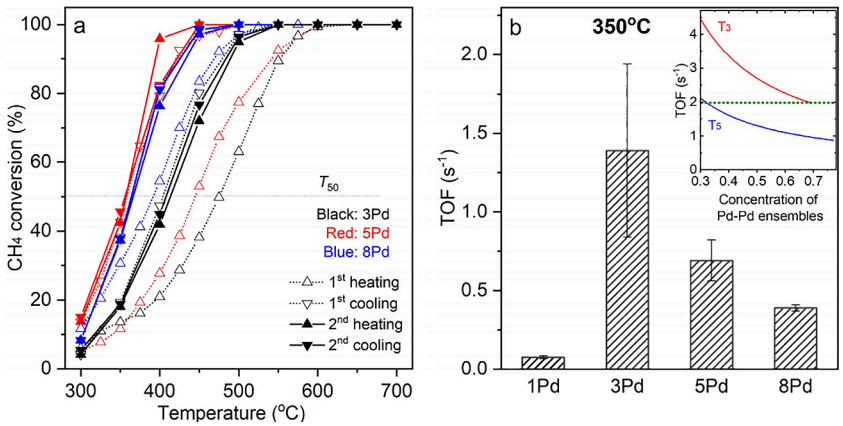

Figure 5. Catalytic properties of Pd-based catalysts for methane combustion. (a) Light-off and light-out curves of CH_4 oxidation over 1Pd, 3Pd, 5Pd and 8 Pd catalysts. Dashed line and open symbol stand for the first reaction cycle, while the solid line and symbol stand for the second reaction cycle. The gas mixture consists of 0.5% CH_4 and 2.5% O_2 in He. (b) TOFs of 1Pd, 3Pd, 5Pd, and 8Pd at 350 °C. The inset shows the estimated range of TOFs of Pd−Pd ensembles in 3Pd (T_3) and 5Pd (T_5) catalysts.

observed Pd−Pd distances in these structures match well with those in the stable Pd−Pd models identified via the theoretical method. This allows us to test the theoretical predictions of the intrinsic activities of the different Pd species. Next, the catalytic properties of these Pd−Pd ensembles in 3Pd and 5Pd are examined and compared with reference single atom and particle counterparts (1Pd and 8Pd).

3.3. High Intrinsic Activity of Pd−Pd Structures. To correlate the structure of Pd species with catalytic properties, we test the as-prepared 3Pd, 5Pd, and 8Pd catalysts for methane combustion at different temperatures (300−700 °C) for two cycles. In each cycle, the heating and subsequent cooling processes are included. As shown in Figure 5a, all three catalysts show improved and stable activities after the first heating process, indicating that the as-prepared catalysts experience structural changes during the first heating process, which is supported by the observations obtained from XPS and XAS. In addition, by combining the results obtained from the activity test, XPS and XAS, it can be concluded that, for the 3Pd and 5Pd catalysts, the produced small Pd−Pd ensembles are responsible for the improved methane conversion, while, for the 8Pd catalyst, the increased activity after the first heating process is most likely correlated with the increased particle size of PdO, as evidenced by the increased coordination numbers of Pd−Pd paths (Table S6). Previous studies also suggested that PdO particles with larger sizes exhibited higher methane combustion activity.[20]

To determine the intrinsic activity of Pd sites in the spent 1Pd, 3Pd, 5Pd, and 8Pd catalysts, the turnover frequencies (TOFs) of all catalysts are obtained by performing SSITKA measurements at 350 °C that allow the tests to be conducted under a kinetically controlled regime. The details of SSITKA measurements and data analysis are in the supporting material (Figures S1 and S2 and Table S7). As shown in Figure 5b, the 3Pd catalyst shows the highest TOF, suggesting that the active species in the 3Pd catalyst has the highest intrinsic activity compared to other catalysts: more than 26 times higher than the single atom 1Pd and 4 times that of PdO in 8Pd. Based on the light-off/-out, XAS, STEM, and XPS results, the Pd species with high intrinsic activities in the spent 3Pd and 5Pd catalysts must be correlated with the Pd−Pd structures formed during the reaction.

To determine the specific intrinsic activity of these Pd−Pd structures, since they coexist with Pd^{4+} and Pd^{2+} single atoms based on the combined XAS, STEM, and XPS, one needs to know the TOFs of Pd^{4+} and Pd^{2+} and their concentrations in the spent 3Pd and 5Pd samples. For the stable Pd^{4+} single atoms, they are embedded in the lattice of ceria supports and thus most likely do not directly participate into the reaction.[28,55] Therefore, we consider that the TOF obtained for the 3Pd (or 5Pd) catalyst is largely contributed by Pd^{2+} single atom sites and Pd^{2+} sites in Pd−Pd ensembles. Among Pd^{2+} single atom and Pd−Pd ensembles, the concentration of Pd−Pd ensembles in 3Pd (5Pd) is estimated to be $0.3 \leq x_3 \leq 0.69$ ($0.3 \leq x_5 \leq 0.77$) and x_3 (x_5) is defined as the concentration of Pd−Pd ensembles in the spent 3Pd (5Pd) catalyst (see Methods for the details of the estimation). Therefore, based on the equations below, we could estimate the TOF of Pd−Pd ensembles in 3Pd (5Pd) catalyst at 350 °C.

$$T_1(1 - x_3) + T_3x_3 = 1.39$$

$$T_1(1 - x_5) + T_5x_5 = 0.69$$

In these equations, 1.39 (0.69) s^{-1} is the TOF of the spent 3Pd (5Pd) catalyst. T_1 (T_3 or T_5) is the TOF of the Pd^{2+} single atom (Pd−Pd ensembles in the 3Pd or 5Pd catalyst). Since the active site in 1Pd catalyst is a Pd^{2+} single atom, T_1 can be obtained from Figure 5b and Table S7 as 0.076 s^{-1}.

As shown in the inset of Figure 5b, which plots the range of T_3 and T_5 as a function of the concentration of Pd−Pd ensembles in the spent 3Pd and 5Pd catalyst, the TOF of Pd−Pd ensembles in the spent 3Pd is estimated to be within the range of $4.5 \geq T_3 \geq 2.0$ s^{-1} and to be within the range of $2.1 \geq T_3 \geq 0.9$ s^{-1} for the Pd−Pd ensembles in the spent 5Pd, much higher than the intrinsic activity of the Pd^{2+} single atom site dominated in the spent 1Pd catalyst and of the PdO nanoparticle dominated in the spent 8Pd catalyst. Chu et al. also reported that neighboring Pd single atoms surpassed isolated single atoms for selective hydrodehalogenation catalysis.[56] In addition, the Pd−Pd ensembles in the spent 3Pd catalyst generally present better activity compared with that in the spent 5Pd catalyst, as suggested by theory.

Obviously, fine-tuning the Pd−Pd distance forming a 2.99-Å Pd_2 structure significantly enhances the intrinsic activity of CH_4 combustion. As confirmed by DFT calculations, such a

https://doi.org/10.1021/acscatal.4c04985
ACS Catal. 2024, 14, 16459−16468

structure is conducive to the formation of oxygen vacancies between the two Pd atoms, which is favorable for the following adsorption and activation of CH_4 and O_2, and hence the facile formation of H_2O and CO_2. One would doubt that the surface defects (such as Ce^{3+} sites and oxygen vacancies) would lead to incorporation of some of the Pd cations in the ceria matrix, and the resulting Pd−Ce interfacial sites would exert additional influence on the intrinsic activity.[11,57,58] In this work, for all of the samples, the catalyst surface displays similar physical and defective properties based on the combined analyses from BET surface area, XRD, Raman, and XPS measurements (Figures S6, S8, and S9 and Table S6). Partial Pd species probably enter the ceria lattice as singly dispersed Pd^{4+}/ Pd^{2+} species (Figure 4b). By comparison, the 1Pd and 3Pd samples show similar Pd−Ce coordination numbers (CNs, Table S6) but quite distinct TOFs: the significantly increased TOF for spent 3Pd is obviously caused by the newly present Pd−Pd structures, as confirmed by the XPS analysis (Figure 4b). For the 5Pd sample, the increased Pd loading leads to the increased formation of Pd−Ce (Table S6) which barely contributes to the activity according to the activity variation between the fresh and spent catalyst until this species reconstructed into 2.75-Å Pd_2 species (Figures 4b and 5). For both spent 3Pd and 5Pd catalysts, the significantly increased activity is accompanied by the transformation of isolated Pd species to Pd_2 structures, whereas further increase of the Pd loading to 8 wt % gives rise to stable Pd^{2+} species-dominated PdO nanoparticles, which show decreased activity than those reconstructed Pd^{4+} species.

4. CONCLUSIONS

In summary, our combined theoretical and experimental results have revealed a Pd−Pd structure that shows high intrinsic activity and atomic efficiency for the reaction of methane combustion. DFT modeling and microkinetic analysis suggest that among various diatomic Pd structures, a stable Pd dimer structure with a 2.99 Å Pd−Pd distance is the most active for methane activation and oxidation. The predicted structure and its superior activity for methane combustion have been confirmed experimentally. This structure was synthesized by tuning the weight loading of Pd on a ceria support and through reaction activation. We found that the TOFs of ceria supported Pd species follow the trend of 2.99 Å Pd−Pd > 2.75 Å Pd−Pd > PdO nanoparticle > Pd single atom. Such agreements allow theory providing insights into the improved catalytic properties of 2.99 Å structure that the high activity of 2.99 Å structure is correlated with the conductive local redox environment from the two O atoms bridging the two Pd^{2+} ions, which facilitates both methane adsorption and activation as well as the production of water and carbon dioxide during the methane oxidation process. Findings from this study hint that confining fully exposed Pd single atoms and controlling their distances or bonding environment can be a potential way to maximize the catalytic CH_4 oxidation activity and the atomic efficiency of precious metals.[59] This work also suggests that the most active Pd species may take only a small portion of all existing species in a heterogeneous Pd catalyst. Maximizing the percentage of the most intrinsically active Pd species will be the focus of our follow-up work.

■ ASSOCIATED CONTENT

Data Availability Statement

The data that support the findings of this study are included in the published article (and its Supporting Information) or available from the corresponding author upon reasonable request.

Supporting Information

The Supporting Information is available free of charge at https://pubs.acs.org/doi/10.1021/acscatal.4c04985.

DFT calculations, SSITKA analysis and additional STEM images, XPS, Raman, XRD, and EXAFS fitting results (PDF)

■ AUTHOR INFORMATION

Corresponding Authors

Yuanyuan Li − *Chemical Sciences Division, Oak Ridge National Laboratory, Oak Ridge, Tennessee 37831, United States;* orcid.org/0000-0003-3074-9672; Email: liy4@ornl.gov

Zili Wu − *Chemical Sciences Division and Center for Nanophase Materials Sciences, Oak Ridge National Laboratory, Oak Ridge, Tennessee 37831, United States;* orcid.org/0000-0002-4468-3240; Email: wuz1@ornl.gov

De-en Jiang − *Interdisciplinary Materials Science and Department of Chemical and Biomolecular Engineering, Vanderbilt University, Nashville, Tennessee 37235, United States;* orcid.org/0000-0001-5167-0731; Email: de-en.jiang@vanderbilt.edu

Authors

Weiwei Yang − *Chemical Sciences Division, Oak Ridge National Laboratory, Oak Ridge, Tennessee 37831, United States; School of Environmental Science and Engineering, Guangdong University of Technology, Guangzhou 510006, People's Republic of China;* orcid.org/0000-0002-9227-0459

Haohong Song − *Interdisciplinary Materials Science, Vanderbilt University, Nashville, Tennessee 37235, United States*

Lihua Zhang − *Center for Functional Nanomaterials, Brookhaven National Laboratory, Upton, New York 11973, United States;* orcid.org/0000-0003-3331-2345

Junyan Zhang − *Chemical Sciences Division, Oak Ridge National Laboratory, Oak Ridge, Tennessee 37831, United States*

Felipe Polo-Garzon − *Chemical Sciences Division, Oak Ridge National Laboratory, Oak Ridge, Tennessee 37831, United States;* orcid.org/0000-0002-6507-6183

Haodong Wang − *Department of Materials Science and Chemical Engineering, Stony Brook University, Stony Brook, New York 11794, United States*

Harry Meyer, III − *Chemical Sciences Division, Oak Ridge National Laboratory, Oak Ridge, Tennessee 37831, United States*

Complete contact information is available at: https://pubs.acs.org/10.1021/acscatal.4c04985

Author Contributions

○W.Y. and H.S. contribute equally to this work. Y.L., Z.W., and D.J. conceived and planned the work. W.Y. and Y.L. synthesized Pd samples, carried out catalytic reactions,

https://doi.org/10.1021/acscatal.4c04985
ACS Catal. 2024, 14, 16459−16468

performed SSITKA measurements, analyzed all collected experimental results, and drafted the manuscript. H.S. and D.J. performed the computational calculations. L.Z. performed the HADDF-STEM measurements. H.W. performed the XAS measurements. H.M. carried out XPS measurements. All of the authors helped in the revision of the manuscript.

Notes

The authors declare no competing financial interest.

■ ACKNOWLEDGMENTS

This research is supported by the U.S. Department of Energy, Office of Science, Office of Basic Energy Sciences, Chemical Sciences, Geosciences, and Biosciences Division, Catalysis Science program. The sample preparation and reaction test were conducted as part of a user project at the Center for Nanophase Materials Sciences, which is a Department of Energy, Office of Science User Facility at Oak Ridge National Laboratory. This research used Hitachi HD2700C STEM of the Center for Functional Nanomaterials (CFN), which is a U.S. Department of Energy Office of Science User Facility, at Brookhaven National Laboratory under Contract No. DE-SC0012704. This research used Beamline 7-BM (QAS) of the National Synchrotron Light Source II, a U.S. Department of Energy (DOE) Office of Science User Facility operated for the DOE Office of Science by Brookhaven National Laboratory under Contract No. DE-SC0012704. This research used resources of the National Energy Research Scientific Computing Center; a DOE Office of Science User Facility supported by the Office of Science of the U.S. Department of Energy under Contract No. DE-AC02-05CH11231. This manuscript has been authored by UT-Battelle, LLC under Contract No. DE-AC05-00OR22725 with the U.S. Department of Energy. The United States Government retains and the publisher, by accepting the article for publication, acknowledges that the United States Government retains a non-exclusive, paid-up, irrevocable, world-wide license to publish or reproduce the published form of this manuscript, or allow others to do so, for United States Government purposes. The Department of Energy will provide public access to these results of federally sponsored research in accordance with the DOE Public Access Plan (http://energy.gov/downloads/doe-public-access-plan).

■ REFERENCES

(1) Tang, Z.; Zhang, T.; Luo, D.; Wang, Y.; Hu, Z.; Yang, R. T. Catalytic Combustion of Methane: From Mechanism and Materials Properties to Catalytic Performance. *ACS Catal.* **2022**, *12* (21), 13457−13474.

(2) He, L.; Fan, Y.; Bellettre, J.; Yue, J.; Luo, L. A review on catalytic methane combustion at low temperatures: Catalysts, mechanisms, reaction conditions and reactor designs. *Renew. Sustain. Energy Rev.* **2020**, *119*, 109589.

(3) Gholami, R.; Alyani, M.; Smith, K. J. Deactivation of Pd Catalysts by Water during Low Temperature Methane Oxidation Relevant to Natural Gas Vehicle Converters. *Catalysts* **2015**, *5* (2), 561−594.

(4) Farrauto, R. J. Low-Temperature Oxidation of Methane. *Science* **2012**, *337*, 659−660.

(5) Cui, Y.; Zhu Chen, J.; Peng, B.; Kovarik, L.; Devaraj, A.; Li, Z.; Ma, T.; Wang, Y.; Szanyi, J.; Miller, J. T.; Wang, Y.; Gao, F. Onset of High Methane Combustion Rates over Supported Palladium Catalysts: From Isolated Pd Cations to PdO Nanoparticles. *J. Am. Chem. Soc. Au* **2021**, *1*, 396−408.

(6) Van den Bossche, M.; Gronbeck, H. Methane Oxidation over PdO(101) Revealed by First-Principles Kinetic Modeling. *J. Am. Chem. Soc.* **2015**, *137* (37), 12035−12044.

(7) Oh, J.; Boucly, A.; van Bokhoven, J. A.; Artiglia, L.; Cargnello, M. Palladium Catalysts for Methane Oxidation: Old Materials. *New Challenges. Acc. Chem. Res.* **2024**, *57* (1), 23−36.

(8) Oh, S. H.; Mitchell, P. J.; Siewert, R. M. Methane oxidation over alumina-supported noble metal catalysts with and without cerium additives. *J. Catal.* **1991**, *132* (2), 287−301.

(9) Lyubovsky, M.; Smith, L. L.; Castaldi, M.; Karim, H.; Nentwick, B.; Etemad, S.; LaPierre, R.; Pfefferle, W. C. Catalytic combustion over platinum group catalysts: fuel-lean versus fuel-rich operation. *Catal. Today* **2003**, *83* (1), 71−84.

(10) Giebeler, L.; Kießling, D.; Wendt, G. $LaMnO_3$ Perovskite Supported Noble Metal Catalysts for the Total Oxidation of Methane. *Chem. Eng. Technol.* **2007**, *30* (7), 889−894.

(11) Chen, S.; Li, S.; You, R.; Guo, Z.; Wang, F.; Li, G.; Yuan, W.; Zhu, B.; Gao, Y.; Zhang, Z.; Yang, H.; Wang, Y. Elucidation of Active Sites for CH_4 Catalytic Oxidation over Pd/CeO_2 Via Tailoring Metal−Support Interactions. *ACS Catal.* **2021**, *11* (9), 5666−5677.

(12) Danielis, M.; Colussi, S.; de Leitenburg, C.; Soler, L.; Llorca, J.; Trovarelli, A. Outstanding Methane Oxidation Performance of Palladium-Embedded Ceria Catalysts Prepared by a One-Step Dry Ball-Milling Method. *Angew. Chem., Int. Ed.* **2018**, *57* (32), 10212−10216.

(13) Senftle, T. P.; van Duin, A. C. T.; Janik, M. J. Role of Site Stability in Methane Activation on $Pd_xCe_{1-x}O_\delta$ Surfaces. *ACS Catal.* **2015**, *5* (10), 6187−6199.

(14) Senftle, T. P.; van Duin, A. C. T.; Janik, M. J. Methane Activation at the Pd/CeO_2 Interface. *ACS Catal.* **2017**, *7* (1), 327−332.

(15) Murata, K.; Kosuge, D.; Ohyama, J.; Mahara, Y.; Yamamoto, Y.; Arai, S.; Satsuma, A. Exploiting Metal−Support Interactions to Tune the Redox Properties of Supported Pd Catalysts for Methane Combustion. *ACS Catal.* **2020**, *10* (2), 1381−1387.

(16) Danielis, M.; Betancourt, L. E.; Orozco, I.; Divins, N. J.; Llorca, J.; Rodríguez, J. A.; Senanayake, S. D.; Colussi, S.; Trovarelli, A. Methane oxidation activity and nanoscale characterization of Pd/CeO_2 catalysts prepared by dry milling Pd acetate and ceria. *Appl. Catal., B* **2021**, *282*, 119567.

(17) Danielis, M.; Colussi, S.; de Leitenburg, C.; Trovarelli, A. The role of palladium salt precursors in $Pd\text{-}PdO/CeO_2$ catalysts prepared by dry milling for methane oxidation. *Catal. Commun.* **2020**, *135*, 105899.

(18) Danielis, M.; Divins, N. J.; Llorca, J.; Soler, L.; Garcia, X.; Serrano, I.; Betancourt, L. E.; Xu, W.; Rodríguez, J. A.; Senanayake, S. D.; Colussi, S.; Trovarelli, A. In situ investigation of the mechanochemically promoted Pd−Ce interaction under stoichiometric methane oxidation conditions. *EES Catal.* **2023**, *1* (2), 144−152.

(19) Yang, W.; Polo-Garzon, F.; Zhou, H.; Huang, Z.; Chi, M.; Meyer, H.; Yu, X.; Li, Y.; Wu, Z. Boosting the Activity of Pd Single Atoms by Tuning Their Local Environment on Ceria for Methane Combustion. *Angew. Chem., Int. Ed.* **2023**, *62* (5), e202217323.

(20) Murata, K.; Ohyama, J.; Yamamoto, Y.; Arai, S.; Satsuma, A. Methane Combustion over Pd/Al2O3 Catalysts in the Presence of Water: Effects of Pd Particle Size and Alumina Crystalline Phase. *ACS Catal.* **2020**, *10* (15), 8149−8156.

(21) Martin, N. M.; Van den Bossche, M.; Hellman, A.; Grönbeck, H.; Hakanoglu, C.; Gustafson, J.; Blomberg, S.; Johansson, N.; Liu, Z.; Axnanda, S.; Weaver, J. F.; Lundgren, E. Intrinsic Ligand Effect Governing the Catalytic Activity of Pd Oxide Thin Films. *ACS Catal.* **2014**, *4* (10), 3330−3334.

(22) Hellman, A.; Resta, A.; Martin, N. M.; Gustafson, J.; Trinchero, A.; Carlsson, P. A.; Balmes, O.; Felici, R.; van Rijn, R.; Frenken, J. W. M.; Andersen, J. N.; Lundgren, E.; Grönbeck, H. The Active Phase of Palladium during Methane Oxidation. *J. Phys. Chem. Lett.* **2012**, *3* (6), 678−682.

https://doi.org/10.1021/acscatal.4c04985
ACS Catal. 2024, 14, 16459−16468

(23) Weaver, J. F.; Hakanoglu, C.; Hawkins, J. M.; Asthagiri, A. Molecular adsorption of small alkanes on a PdO(101) thin film: Evidence of σ-complex formation. *J. Chem. Phys.* **2010**, *132* (2), No. 024709.
(24) Antony, A.; Asthagiri, A.; Weaver, J. F. Pathways and kinetics of methane and ethane C−H bond cleavage on PdO(101). *J. Chem. Phys.* **2013**, *139* (10), 104702.
(25) Chen, J.; Zhong, J.; Wu, Y.; Hu, W.; Qu, P.; Xiao, X.; Zhang, G.; Liu, X.; Jiao, Y.; Zhong, L.; Chen, Y. Particle Size Effects in Stoichiometric Methane Combustion: Structure−Activity Relationship of Pd Catalyst Supported on Gamma-Alumina. *ACS Catal.* **2020**, *10* (18), 10339−10349.
(26) Murata, K.; Mahara, Y.; Ohyama, J.; Yamamoto, Y.; Arai, S.; Satsuma, A. The Metal-Support Interaction Concerning the Particle Size Effect of Pd/Al_2O_3 on Methane Combustion. *Angew. Chem., Int. Ed.* **2017**, *56* (50), 15993−15997.
(27) Su, Y. Q.; Liu, J. X.; Filot, I. A. W.; Zhang, L.; Hensen, E. J. M. Highly Active and Stable CH(4) Oxidation by Substitution of Substitution of Ce^{4+} by Two Pd^{2+} Ions in CeO_2(111). *ACS Catal.* **2018**, *8* (7), 6552−6559.
(28) Wei, Y.; Zhang, Y.; Zhang, P.; Xiong, J.; Mei, X.; Yu, Q.; Zhao, Z.; Liu, J. Boosting the Removal of Diesel Soot Particles by the Optimal Exposed Crystal Facet of CeO_2 in Au/CeO_2 Catalysts. *Environ. Sci. Technol.* **2020**, *54* (3), 2002−2011.
(29) Xiong, H.; Kunwar, D.; Jiang, D.; García-Vargas, C. E.; Li, H.; Du, C.; Canning, G.; Pereira-Hernandez, X. I.; Wan, Q.; Lin, S.; Purdy, S. C.; Miller, J. T.; Leung, K.; Chou, S. S.; Brongersma, H. H.; ter Veen, R.; Huang, J.; Guo, H.; Wang, Y.; Datye, A. K. Engineering catalyst supports to stabilize PdO_x two-dimensional rafts for water-tolerant methane oxidation. *Nat. Catal.* **2021**, *4* (10), 830−839.
(30) Ta, N.; Liu, J.; Chenna, S.; Crozier, P. A.; Li, Y.; Chen, A.; Shen, W. Stabilized Gold Nanoparticles on Ceria Nanorods by Strong Interfacial Anchoring. *J. Am. Chem. Soc.* **2012**, *134* (51), 20585−20588.
(31) Ravel, B.; Newville, M. ATHENA, ARTEMIS, HEPHAESTUS: data analysis for X-ray absorption spectroscopy using IFEFFIT. *J. Synchrotron Radiat.* **2005**, *12* (4), 537−541.
(32) Liu, D.; Li, Y.; Kottwitz, M.; Yan, B.; Yao, S.; Gamalski, A.; Grolimund, D.; Safonova, O. V.; Nachtegaal, M.; Chen, J. G.; Stach, E. A.; Nuzzo, R. G.; Frenkel, A. I. Identifying Dynamic Structural Changes of Active Sites in Pt−Ni Bimetallic Catalysts Using Multimodal Approaches. *ACS Catal.* **2018**, *8* (5), 4120−4131.
(33) Frenkel, A. I. Applications of extended X-ray absorption fine-structure spectroscopy to studies of bimetallic nanoparticle catalysts. *Chem. Soc. Rev.* **2012**, *41* (24), 8163−8178.
(34) Li, Y.; Rehr, J. J.; Nuzzo, R. G.; Frenkel, A. I. Nanoclusters. *International Tables for Crystallography*; International Tables Online, 2022; Vol. *I*. DOI: 10.1107/S1574870720004723.
(35) Li, Y.; Frenkel, A. I., Metal Nanocatalysts. In *XAFS Techniques for Catalysts, Nanomaterials, and Surfaces*; Iwasawa, Y., Asakura, K., Tada, M., Eds.; Springer International: Cham, Switzerland, 2017; pp 273−298. DOI: 10.1007/978-3-319-43866-5_19.
(36) Wang, X.; Shi, H.; Szanyi, J. Controlling selectivities in CO_2 reduction through mechanistic understanding. *Nat. Commun.* **2017**, *8* (1), 513.
(37) Polo-Garzon, F.; Pakhare, D.; Spivey, J. J.; Bruce, D. A. Dry Reforming of Methane on Rh-Doped Pyrochlore Catalysts: A Steady-State Isotopic Transient Kinetic Study. *ACS Catal.* **2016**, *6* (6), 3826−3833.
(38) Kresse, G.; Furthmüller, J. Efficiency of ab-initio total energy calculations for metals and semiconductors using a plane-wave basis set. *Comput. Mater. Sci.* **1996**, *6* (1), 15−50.
(39) Kresse, G.; Furthmüller, J. Efficient iterative schemes for ab initio total-energy calculations using a plane-wave basis set. *Phys. Rev. B* **1996**, *54* (16), 11169−11186.
(40) Perdew, J. P.; Burke, K.; Ernzerhof, M. Generalized Gradient Approximation Made Simple. *Phys. Rev. Lett.* **1996**, *77* (18), 3865−3868.
(41) Fabris, S.; de Gironcoli, S.; Baroni, S.; Vicario, G.; Balducci, G. Reply to "Comment on 'Taming multiple valency with density functionals: A case study of defective ceria'". *Phys. Rev. B* **2005**, *72* (23), 237102.
(42) Wu, T.; Vegge, T.; Hansen, H. A. Enhanced activity for electrocatalytic H2 production through cooperative Pr and Bi co-doping of CeO_2 in solid oxide electrolysis cells. *J. Catal.* **2021**, *402*, 310−314.
(43) Li, Y.; Wang, H.; Song, H.; Rui, N.; Kottwitz, M.; Senanayake, S. D.; Nuzzo, R. G.; Wu, Z.; Jiang, D.-e.; Frenkel, A. I. Active sites of atomically dispersed Pt supported on Gd-doped ceria with improved low temperature performance for CO oxidation. *Chem. Sci.* **2023**, *14* (44), 12582−12588.
(44) Kresse, G.; Joubert, D. From ultrasoft pseudopotentials to the projector augmented-wave method. *Phys. Rev. B* **1999**, *59* (3), 1758−1775.
(45) Blöchl, P. E. Projector augmented-wave method. *Phys. Rev. B* **1994**, *50* (24), 17953−17979.
(46) Henkelman, G.; Uberuaga, B. P.; Jónsson, H. A climbing image nudged elastic band method for finding saddle points and minimum energy paths. *J. Chem. Phys.* **2000**, *113* (22), 9901−9904.
(47) Henkelman, G.; Jónsson, H. A dimer method for finding saddle points on high dimensional potential surfaces using only first derivatives. *J. Chem. Phys.* **1999**, *111* (15), 7010−7022.
(48) Filot, I.; Zijlstra, B.; Hensen, E. MKMCXX, a C++ program for constructing microkinetic models. *SCM*, 2012.
(49) Stegelmann, C.; Andreasen, A.; Campbell, C. T. Degree of rate control: how much the energies of intermediates and transition states control rates. *J. Am. Chem. Soc.* **2009**, *131* (23), 8077−8082.
(50) Campbell, C. T. The Degree of Rate Control: A Powerful Tool for Catalysis Research. *ACS Catal.* **2017**, *7* (4), 2770−2779.
(51) Song, B.; Si, S.; Soleymani, A.; Xin, Y.; Hagelin-Weaver, H. E. Effect of ceria surface facet on stability and reactivity of isolated platinum atoms. *Nano Res.* **2022**, *15* (7), 5922−5932.
(52) Kwak, J. H.; Hu, J.; Mei, D.; Yi, C.-W.; Kim, D. H.; Peden, C. H. F.; Allard, L. F. A.; Szanyi, J. Coordinatively Unsaturated Al^{3+} Centers as Binding Sites for Active Catalyst Phases of Platinum on g-Al_2O_3. *Science* **2009**, *325*, 1670−1673.
(53) Muravev, V.; Spezzati, G.; Su, Y.-Q.; Parastaev, A.; Chiang, F.-K.; Longo, A.; Escudero, C.; Kosinov, N.; Hensen, E. J. M. Interface dynamics of $Pd-CeO_2$ single-atom catalysts during CO oxidation. *Nat. Catal.* **2021**, *4* (6), 469−478.
(54) Gulyaev, R. V.; Kardash, T. Y.; Malykhin, S. E.; Stonkus, O. A.; Ivanova, A. S.; Boronin, A. I. The local structure of $Pd_xCe_{1-x}O_{2-x-delta}$ solid solutions. *Phys. Chem. Chem. Phys.* **2014**, *16* (26), 13523−13539.
(55) Su, Y.-Q.; Filot, I. A. W.; Liu, J.-X.; Hensen, E. J. M. Stable Pd-Doped Ceria Structures for CH4 Activation and CO Oxidation. *ACS Catal.* **2018**, *8* (1), 75−80.
(56) Chu, C.; Huang, D.; Gupta, S.; Weon, S.; Niu, J.; Stavitski, E.; Muhich, C.; Kim, J.-H. Neighboring Pd single atoms surpass isolated single atoms for selective hydrodehalogenation catalysis. *Nat. Commun.* **2021**, *12* (1), 5179.
(57) Lei, Y.; Li, W.; Liu, Q.; Lin, Q.; Zheng, X.; Huang, Q.; Guan, S.; Wang, X.; Wang, C.; Li, F. Typical crystal face effects of different morphology ceria on the activity of Pd/CeO_2 catalysts for lean methane combustion. *Fuel* **2018**, *233*, 10−20.
(58) Yang, K.; Wang, K.; Shen, X.; Zhang, F.; Huang, B.; Yan, K.; Shi, Y.; He, Y.; Xie, P. Ceria crystal facet impact for methane C−H activation in Pd/CeO_2 catalysts. *Catal. Sci. Technol.* **2023**, *13* (15), 4489−4497.
(59) Chen, Y.; Lin, J.; Pan, Q.; Liu, X.; Ma, T.; Wang, X. Inter-Metal Interaction of Dual-Atom Catalysts in Heterogeneous Catalysis. *Angew. Chem., Int. Ed.* **2023**, *62* (42), No. e202306469.

https://doi.org/10.1021/acscatal.4c04985
ACS Catal. 2024, 14, 16459−16468